AIAA AVIATION Forum
12-16 June 2023, San Diego, CA and Online
AIAA aviation 2023 Forum

10.2514/6.2023-4059

Development of a Model-Driven Calibration Method for Remote Microphone Probes Using Bayesian Inference

Olivier Moriaux* and Riccardo Zamponi†
von Karman Institute for Fluid Dynamics, 1640 Sint-Genesius-Rode, Flemish Brabant, Belgium
Delft University of Technology, 2629HS Delft, South Holland, The Netherlands

Christophe Schram‡
von Karman Institute for Fluid Dynamics, 1640 Sint-Genesius-Rode, Flemish Brabant, Belgium

Unsteady surface pressures shed light on the turbulent structures of boundary-layer flows, which dictate for a large part the aerodynamic and aeroacoustic performance of bodies submersed in a flow. Remote microphone probes (RMP) provide advantages compared to flush-mounted probes because of their reduced sensing area. However, they feature a distinct transfer function (TF) that needs to be taken into account for accurate pressure measurements. The empirical calibration of the probes, e.g., using plane-wave tubes, can introduce spurious resonant frequencies into the TF due to a lack of control of the pressure field inside the calibrator over the multiple calibration steps. Current processing methods of calibration data tend to be manual and strongly related to the operator's expertise. Depending on the processing, spurious resonance may remain in a given frequency band, or some resonance that is characteristic of the probe may wrongfully be removed. All errors in the TF inadvertently propagate to the measurements performed with the calibrated probe. In this study, a semi-empirical calibration method is proposed with the aim of removing the spurious resonance in a physics-driven manner that is less reliant on the operator. Bayesian inversion is used to fit an analytic model for the TF of the RMP to the empirical calibration data. An inviscid acoustic finite-element method (FEM) simulation serves as a benchmark dataset. As such, the semi-empirical calibration procedure can be tested in an idealized environment.The proposed method is shown to be capable of providing a highly accurate fit to the benchmark data, with much less operator intervention than current processing methods. Its application to experimental calibration data and wall-pressure measurements appears to be a feasible next step, which is bound to show the full promise and potential of the technique.

I. Nomenclature

A	=	Tube cross-sectional area, m^2
α	=	Shear wavenumber, -
$\hat{\alpha}$	=	Thermal diffusivity, $m^2\,s^{-1}$
$\bar{\alpha}$	=	Model/system parameter vector
c	=	Speed of sound, $m\,s^{-1}$
d	=	Measurements vector
ε	=	Measurement error vector
f	=	Frequency, Hz
$\mathscr{F}$	=	Fourier-transform operator
γ	=	Ratio of specific heats, -
H	=	Observation operator
i	=	Index of parallel tube-transducer nodes
j	=	Index of serial tube-transducer nodes
J_k	=	Bessel function of the first kind of order k
k_L	=	Reduced frequency (length), -
L	=	Tube length, m
m	=	Model operator
μ	=	Dynamic viscosity, Pa s
n	=	Polytropic exponent, -
ν	=	Kinematic viscosity, $m^2\,s^{-1}$
ω	=	Angular frequency, $rad\,s^{-1}$
p	=	Pressure signal, Pa
Pr	=	Prandtl number, -
Φ	=	Branch complex impedance, -
ϕ	=	Wave propagation factor, m^{-1}

*Short Training Program fellow, Environmental and Applied Fluid Dynamics dept, olivier.moriaux@vki.ac.be
†Research Professor, Environmental and Applied Fluid Dynamics, riccardo.zamponi@vki.ac.be, AIAA Member.
‡Professor, Environmental and Applied Fluid Dynamics / Aeronautics and Aerospace depts, christophe.schram@vki.ac.be, AIAA Member.

$\overline{\overline{P}}$ = Sampling Gaussian covariance matrix
R = Tube radius, m
ρ = Probability density function (PDF)
ρ_s = Density, kg m^{-3}
$\overline{\overline{R}}$ = Measurement error matrix
$S_{x,y}$ = Cross-power-spectral density between signal x and y
$\overline{\sigma}_d$ = Measurement error standard deviation vector
u = Model/System State vector
$\overline{U}_{tunnel}$ = Mean flow velocity in the outer flow region above the pressure measurement port, m s^{-1}
V_e = Effective volume, m^3
V_t = Tube volume, m^3
V_v = Cavity volume, m^3

II. Introduction

Unsteady wall-pressure measurements are often acquired in the field of experimental aerodynamics. Surface pressures determine the steady and unsteady forces that act upon a body submerged in flow [1]. The chordwise distribution of these unsteady pressures serves as a footprint of the flow over the surface, e.g., separation bubbles [2]. The surface pressure fluctuations can be linked to turbulent structures within the boundary layer [3] and are one of the primary sources of noise production of bodies immersed in a flow [4].

Many techniques exist to measure surface pressures, ranging from the classical U-tube manometers [5] to the novel pressure-sensitive paints [6]. Nevertheless, due to their fast response and accuracy, the conventional apparatuses used for unsteady pressure measurements are typically microphones. These can be either flush-mounted on the surface, installed inside a cavity behind a pinhole on the surface, or mounted inside a cavity connected to the surface pinhole through a system of tubes. Flush mounting the transducer allows for direct measurement of the pressure in the region of interest. Thus, only the transducer must be calibrated to accurately measure the surface pressure.

The large sensing area of the flush-mounted transducer results in an averaging of high-frequency turbulent pressure fluctuations with wavelengths of similar size to or larger than the sensing area. Corcos [7] provides a method to correct several derived quantities of the pressure fluctuations for specific inflow conditions. By minimizing the sensing area, the correction factor can be strongly reduced, decreasing the possible inaccuracies introduced by the assumptions of Corcos' method. Additionally, decreasing the sensing areas makes it possible to position the sensors closer to each other, improving derived flow quantities such as correlation length and convection speed. For this reason, the sensor is often placed in a small cavity directly underneath a pinhole on the surface. However, the pinhole and transducer cavity geometries result in internal reflections since the geometry acts as a Helmholtz resonator. If the resonance frequency of the pinhole is high enough, the pinhole will have little to no effect on the pressure signal that enters the system and is measured by the transducer. Mounting the microphone remotely within a system of volumes and tubes allows placing the transducer even further from the surface than with a conventional pinhole design. This solution is beneficial for models with little internal volume. Nevertheless, a transducer placed directly behind a pinhole or located remotely from the testing geometry measures pressure fluctuations that differ from those on the surface due to viscous effects and acoustic wave reflections within the narrow passages. Thus, a remote setup requires additional calibration, apart from the aforementioned transducer calibration, to counteract the signal transformation that it brings [8]. With the transfer function (TF) that results from the calibration process, the signal measured by the sensor can be converted into the pressure fluctuations on the surface. The TF of a system is a measure of how it amplifies and delays pressure fluctuations at varying frequencies.

Analytic models for the frequency response of pneumatic systems [9–15], based on simplified governing equations for the internal flow field of the system, can be used as a tool with which the RMP can be designed for favorable frequency response, e.g., by counteracting saturation of the transducer with the damping effect of the RMP. However, the analytical approach tends not to be used for the calibration of probes as it requires exact knowledge of the geometry of the system and the properties of the internal flow. The effective dimensions can be different due to production or assembly inaccuracies, e.g., the additional cavity volume created by the microphone membrane protection grid. Additionally, these models only account for the TF of the tubes and cavities, which does not include any TF imposed by the microphone or the gain of the pressure-measurement system. For a complete TF of the real-world system, an empirical part of the calibration procedure is still required. Hence, the conventional way of calibrating pressure measurement systems is with empirical frequency-domain dynamic calibration methods [5, p.70]. The methods rely on a few assumptions compared to analytic frequency-response models. They are relatively straightforward to perform and account for the TF of the full pressure measurement system, i.e., the RMP geometry and the transducer itself.

The empirical frequency-domain dynamic calibration processes [5, p.70] works by exciting the RMP and a flush-mounted reference microphone with a known TF with the same pressure fluctuation source. In doing so, the

frequency response of the RMP can be related to the known frequency response of the reference microphone, in one or more calibration steps, e.g., [16–18]. A plane-wave calibrator, such as shown in Fig. 3 and [16], may not be able to fit both a flush-mounted reference microphone *'ref.'* and a RMP in a single calibration step. In such a case, two or more calibration steps are required using a microphone mounted within the calibrator *'cal.'* as an intermediary signal to link the calibration steps together. From the data from both calibration steps, Eq. (1) can be used to estimate the TF of the RMP.

$$TF_{\mathrm{RMP}\to\mathrm{ref.}}(f) = \frac{S_{\mathrm{ref.,\,RMP}}(f)}{S_{\mathrm{RMP,\,RMP}}(f)} = \frac{\mathscr{F}\left[p'_{\mathrm{ref.}}\right]}{\mathscr{F}\left[p'_{\mathrm{RMP}}\right]} = \underbrace{\frac{\mathscr{F}\left[p'_{\mathrm{ref.}}\right]}{\cancel{\mathscr{F}\left[p'_{\mathrm{cal.}}\right]}}}_{TF_{\mathrm{cal.}\to\mathrm{ref.}}} \underbrace{\frac{\cancel{\mathscr{F}\left[p'_{\mathrm{cal.}}\right]}}{\mathscr{F}\left[p'_{\mathrm{RMP}}\right]}}_{TF_{\mathrm{RMP}\to\mathrm{cal.}}} \tag{1}$$

However, two major problems can be found with the empirical calibration process: (i) the calibrator equipment itself is a tube-volume system that can introduce resonant frequencies into the final TF; (ii) the calibration conditions often do not reflect the conditions when the RMP is in use, e.g., immersed in a grazing flow or high-temperature environments. The first of these problems is the most notable. These methods require two or more steps to relate the response of a remote microphone probe (RMP) to the response of a flush-mounted microphone. As noted by Van de Wyer et al. [16], combining different TFs in Eq. (1) results in errors in the final TF when the pressure field inside the calibrator is not the same between these calibration steps. Resonance linked to the calibrator geometry does not cancel out in the combined TF when the resonance in both steps results from a different pressure field.

In the case depicted above, manual tweaking of TFs becomes necessary not to introduce errors in the unsteady wall-pressure measurements. Examples of such a process include splicing TFs that use different signals and smoothing the result [16], or combining TFs from many different calibrations [19]. However, this task requires a thorough understanding of the expected frequency response of the RMP. Indeed, the tweaking can introduce new errors or overlook a spurious frequency response as characteristic of the probe.

In view of the above, a new calibration post-processing technique that (i) reduces the operator dependence on the calibration results and (ii) ideally considers the physics behind the TF of the probe during the data processing is currently needed. The idea of the present research is to fill this gap and develop a semi-empirical calibration method that uses analytical techniques, such as those developed by Whitmore [13], to remove calibrator geometry-induced resonant frequencies from empirically-obtained TFs.

Bayesian inference (BI) is used to couple the analytical model to the calibration data instead of a simple curve-fitting method. Whereas the latter fitting method will adapt the model parameters as long as it minimizes the difference between the model TF and calibration data, BI also considers the likelihood of those parameter values. In doing so, BI prioritizes good-fitting solutions that result from feasible parameter values. As such, the BI method offers great results when using real data with measurement errors that come from a system of which the operator has some prior knowledge [20–22], e.g., an estimate of the geometrical dimensions of the RMP. By fitting the analytical model to the calibration data, all resonance and attenuation are present in the model TF, while any resonance that cannot be reproduced by the model for feasible parameter values under the model physics is not included in the model TF.

In this regard, calibration data generated by an acoustic finite element method (FEM) simulation can serve as a preliminary validation of this new method. The FEM simulation dataset offers a controlled environment that can be used to build the method from the ground up and assess its feasibility.

The preliminary results achieved in the initial testing of the proposed method are presented in this paper. The outcome of the investigation shows that the calibration post-processing method is capable of providing a TF fit that contains all the resonant frequencies, as well as matching the amplitude and phase outside of frequency bands that are affected by spurious inviscid resonance. As a result, the method not only removes spurious resonance with little operator intervention but is also capable of replacing the affected frequency band of the TF with a physically-correct alternative. Although further testing will be needed on real plane-wave data to confirm these findings, the proposed method represents a promising approach to improving current calibration techniques for pressure transducers.

The importance of both pressure measurements and the associated calibration of the pressure probes have been stated in this introduction. The theory of the models used for the proposed method is briefly reviewed in Section III. The details of the implementation of the theoretical models into the semi-empirical method and the generation of the numerical FEM dataset are outlined in Section IV. In Section V, the proposed method is benchmarked against the dataset. The application of the technique to real calibration data and its extension with a-posteriori correction terms are also discussed here. Finally, the paper's findings are summarized in Section VI.

III. Theory: Description of the semi-empirical calibration method

The theory at the basis of the proposed semi-empirical calibration method is summarized in this section. First, the analytical model of Whitmore [13], used to describe the TF of a pinhole probe with varying parameters of the tubes, is mentioned in Section III.A. Lastly, the statistical framework of the Bayesian inference (BI) and the employed Markov chain Monte Carlo (McMC) method, which are used to couple the aforementioned theoretical model to the calibration data, are explained in Section III.B.

A. Tube-transducer model

The Whitmore [13] (W) model is chosen for the method proposed in this research for the following reasons: (i) similarly to the model of Bergh and Tijdeman [11], it discretizes the RMP geometry in tube-cavity elements, which makes it easy to set up for any geometry. Yet, in comparison to the aforementioned model, (ii) it allows branching geometries, which are indispensable for the semi-infinite waveguide type RMPs that consist of a primary channel with an anechoic termination and a side-branch containing the transducer [8]. As mentioned by the author of this model, it functions in a similar way to Kirchoff's laws by building an equivalent serial tube-transducer system from parallel geometries using the concept of complex equivalent volumes V_e for the transducer cavity. The model accounts for the impact of downstream elements on the considered tube-cavity element by reducing these elements into a complex-valued cavity volume, see Fig. 1. Both serial and parallel nodes use the same equation for effective volume, as a serial node is simply a parallel node with a single branch.

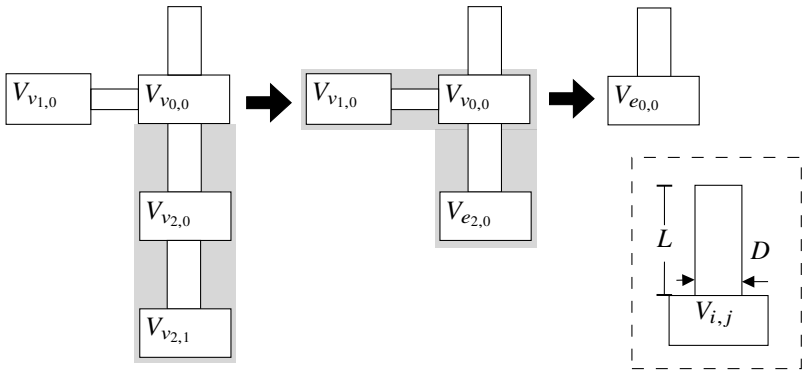

Fig. 1 Illustration of the reduction of a parallel pneumatic system geometry to a serial geometry with the W model. Tube-transducer elements have a coordinate (i, j), where i is used to denote parallel branches, and j denotes the serial element in the branch. Grey areas illustrate regions reduced to e ective volume in the next step.

The W model equations presented below use the parameter definitions of Bergh and Tijdeman [11] to allow for easy comparison with this model:

$$\frac{p_j}{p_{j-1}} = \left[\cosh\langle\phi_j L_j\rangle + \frac{V_{e_j}}{V_{t_j}}\phi_j L_j \sinh\langle\phi_j L_j\rangle\right]^{-1}; \quad \left(\frac{V_e}{V_t}\right)_j = \left(\frac{V_v}{V_t}\right)_j \left[1 + \sum_{i=1}^{N} \Phi_{i,j}\right]; \quad V_{e_N} = V_{v_N};$$
$$\Phi_{i,j} = \frac{V_{t_i}}{V_{v_j}} \left(\frac{V_e}{V_t}\right)_i \left(\frac{c_j}{c_i}\right)^2 \frac{\cosh\langle\phi_i L_i\rangle + \sinh\langle\phi_i L_i\rangle / [\phi_i L_i (V_e/V_t)_i]}{\cosh\langle\phi_i L_i\rangle + \sinh\langle\phi_i L_i\rangle \cdot [\phi_i L_i (V_e/V_t)_i]}; \quad \text{For serial node: } i = j + 1; \tag{2}$$
$$\phi_j L_j = \frac{\omega L_j}{c_j}\sqrt{\frac{J_0\langle\alpha_j\rangle}{J_2\langle\alpha_j\rangle}}\sqrt{\frac{\gamma}{n_j}}; \qquad \alpha_j = i^{3/2} R_j \sqrt{\frac{\rho_{s_j}\omega}{\mu_j}}; \qquad n_j = \left[1 + \frac{\gamma - 1}{\gamma}\frac{J_2\langle\alpha_j\sqrt{P_r}\rangle}{J_0\langle\alpha_j\sqrt{P_r}\rangle}\right]^{-1}.$$

As the model is used to fit onto data, its variables are used and presented in a non-dimensionalized form. In doing so, parameters with a similar effect on the system are combined, such that each non-dimensionalized parameter impacts the physics of the TF of the RMP in a unique way. By grouping together variables that only appear in combination with certain other parameters, e.g., V_e/V_t, and based on the work of Tijdeman [23], the normalized model parameters of

Eq. (3) are considered.

$$k_{L,j} = \frac{\omega L_j}{c_j}; \qquad \alpha_j = i^{3/2} R_j \sqrt{\frac{\omega}{\nu_j}}; \qquad \left(\frac{V_v}{V_t}\right)_j = \frac{V_{v_j}}{L_j \pi R_j^2};$$
$$\gamma_j = \left(\frac{c_p}{c_v}\right)_j; \qquad Pr_j = \left(\frac{\nu}{\hat{\alpha}}\right)_j; \qquad \frac{V_{t_i}}{V_{v_j}} = \frac{L_i \pi R_i^2}{V_{v_j}}; \qquad \frac{c_i}{c_j} = \sqrt{\frac{\gamma_i R_i T_i}{\gamma_j R_j T_j}}. \tag{3}$$

For a single tube-cavity element, i.e., a pinhole-type RMP, three main geometrical parameters remain. First, the reduced frequency affects the line resonance, as can be understood by relating it to the line resonance equations, such as for open-ended tubes:

$$f_{r,t} = \frac{c}{2L} \cdot n \quad \text{with } n \in \mathbb{N}_1 \quad \rightarrow \quad n\pi = \frac{2\pi f_{r,t} L}{c} = \frac{\omega L}{c} = k_L. \tag{4}$$

Second, the reduced frequency together with the shear wavenumber affects the viscous attenuation of the pressure waves traveling through the tube. As α contains the kinematic viscosity, it affects the overall viscosity within the tube and cavity. Finally, the parameter V_v/V_t affects the cavity resonance of the tube-cavity section, as can be seen by considering the equation for a Helmholtz resonator:

$$f_c = \frac{c}{2\pi}\sqrt{\frac{A}{V_v L}} = \frac{c}{2\pi L}\sqrt{\frac{V_t}{V_v}} \quad \rightarrow \quad k_{L,c} = \frac{2\pi f_c L}{c} = \left(\frac{V_v}{V_t}\right)^{-1/2}. \tag{5}$$

The W model does have some limitations, which are linked to the linearization of the Navier-Stokes equations and the assumptions used to simplify them. The model assumes that the longitudinal wave expansion process inside of the tubes is polytropic. The flow within the tube is one-dimensional, which requires high-aspect-ratio tubes $L/R > 20$ [24]. Gas properties are invariant over each tube section but are allowed to differ between two tube-cavity elements. The tube cavity has a negligible length with respect to the tube length. The pressure-wave amplitudes in the tube-cavity system need to be small to allow for the assumption of small perturbations needed for the linearization and for the assumption of laminar flow. For this, Gumley [24] provides the following equation as a pointer for the validity of this assumption:

$$L \Big/ \left(R^3 \overline{U}^2_{tunnel}\right) > 1.6 \times 10^6 \, \mathrm{s}^2 \, \mathrm{m}^{-4}. \tag{6}$$

Yet, the model for the wave propagation factor poses additional limitations Tijdeman [23]:

$$\frac{R}{L} \cdot k_L \ll 1 \text{ and } \frac{R}{L} \cdot k_L \Big/ |\alpha| \ll 1.$$

As mentioned in Section II, several other limitations inhibit these analytical models from being used for the purpose of calibrating RMPs. In order to accurately determine the model TF, the exact dimensions of the RMP need to be known. Any inaccuracy in the dimensions provided to the model results in a different TF. Small differences in the geometry can easily result from production or assembly inaccuracies or other unforeseen aspects, e.g., the additional cavity volume introduced by the volume between the protection grid and membrane of a microphone. In addition, these models only account for the TF of the tubes and cavities, not the gain of the acquisition system or the characteristic TF of the specific microphone. Therefore, to determine the TF of a RMP, any calibration procedure must contain an empirical part, at least for validation of the model TF. Using BI, introduced in Section III.B, the model parameters can be inferred from the empirical calibration data.

B. Bayesian inference

The second part of the analytic aspect of the semi-empirical calibration method is the BI method, which serves to couple the analytical model for the tube-transducer system to its empirical calibration data. Both the model and real RMP can be defined by a set of parameters, e.g., the W model parameters in Eq. (3). Considering the physics behind the propagation of the pressure-fluctuation waves through the RMP, summarized by the W model, for a given set of parameter values, the system state of the RMP is defined. Through empirical calibration or modeling the TF at certain frequencies, the system state is sampled with some additional measurement error. This is equivalent to following the process in Fig. 2 from left to right. If the measurement error is considered a random variable, then the output for a given

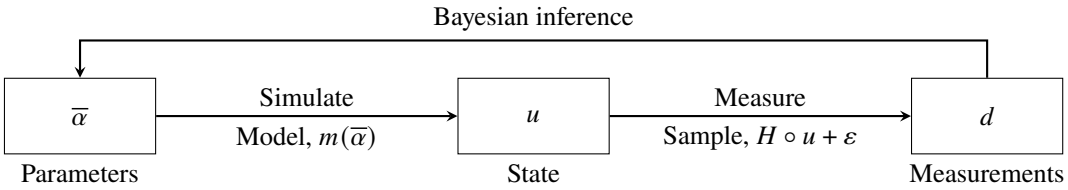

Fig. 2 BI concept schematic.

set of parameter values is a PDF for each measurement. If empirical calibration data are available, the probability of observing that TF can be defined, given the assumed parameter values.

A similar PDF can be computed if many empirical calibrations of the same probe are performed. Then by iterating over parameter values through the left to the right process of Fig. 2, one can match the model measurement PDF to the observed measurement PDF. In doing so, one infers the parameter values from measurement data and a representative system model. This is called Bayesian inference. Several implementations of BI exist, yet they all rely on three PDFs: the prior, the likelihood, and the posterior [25].

Each parameter value has a probability of occurring. This is termed the prior PDF $\rho_0(\overline{\alpha})$ and is formed from the prior knowledge and assumptions of the operator. For example, if the cavity volume is dependent on the specific mounting of the microphone to the RMP, then it will have a range of attainable values characterized by a mean and a variance, and possibly other statistical moments. A PDF summarizing the plausible cavity volumes can be defined simply based on a CAD file, or further refined by measurement of the volume [11].

The likelihood PDF $\rho(d|\overline{\alpha})$ defines the probability of the observed measurements being a result of the system state, defined by the set of parameters $\overline{\alpha}$. This PDF is based on the deviation of the measurements from the state, sampled at the same coordinates as the measurements using the observation operator. Here the measurement error is defined as an independent and identically distributed multi-variate Gaussian with zero mean and covariance $\overline{\overline{R}}$:

$$d - H \circ m(\overline{\alpha}) = \varepsilon \sim \mathcal{N}(\overline{0}, \overline{\overline{R}}) \qquad \text{with } \overline{\overline{R}} = \overline{\sigma}_d^2 \overline{\overline{I}}. \tag{7}$$

The posterior $\rho(\overline{\alpha}|d)$ combines both of these knowledge sources: the prior knowledge of the system, and the knowledge provided by the model fit on the data:

$$\rho(\overline{\alpha}|d) \sim \rho(d|\overline{\alpha}) \cdot \rho_0(\overline{\alpha}).$$

The form presented here is not normalized by the evidence $\rho(d)$ as explained further by Skilling [20, p.6]. Since the objective is to find the RMP parameter values that are most likely to result in the empirical calibration data, the idea is to find the absolute maximum of the posterior, termed the maximum a posteriori (MAP).

Provided that the model closely reflects the physics affecting the real system from which measurements are taken, the model TF using the MAP-parameters fit should perfectly reflect the measurements. In this case, the TF is expected to contain all relevant attenuation, delay, and resonance, ignoring the effects that are not producible by the considered RMP system and its physics. This means that calibrator-induced imperfections in a multi-stage calibration are smoothed over, and minor errors in the dimensions of the RMP are accounted for, thus fulfilling the main objective of the semi-empirical calibration method. The crux of the problem then lies in assessing whether or not the chosen model is capable of providing a satisfactory fit of the measurements and finding the optimal fit of the model with the data, i.e., the MAP.

Finding the MAP does not pose an issue for linear models with a Gaussian prior as they have a closed-form solution for the posterior [26]. For non-linear models, such as the W model, the MAP can only be found by iteratively sampling the posterior. Each sample of the posterior in requires the model to be evaluated for the new parameter values, which can become computationally expensive. Various BI implementations exist with the goal of finding an estimate of the MAP, and sometimes also estimating the posterior PDF, in a computationally efficient way. Two types of implementations were considered in this case: the gradient-ascent method and the McMC method*.

The chosen implementation is the Metropolis-Hastings (MH) version of the McMC [27] due to several advantages it holds over the gradient-ascent with the adjoint method. First, the implementation of MH is much less involved than that of a gradient-ascent method. Second, the random sampling of the MH algorithm does not only converge to the MAP but

*Dwight, R. P., "Uncertainty Quantification: Propagation and inversion in complex models," https://aerodynamics.lr.tudelft.nl/~rdwight/cfdiv/index.html, Apr. 2022. Accessed on: 26/04/2023.

also samples around this region of high probability. These samples can be used to provide an estimate of the posterior PDF. This allows the proposed calibration method also to give an estimate of the uncertainty of MAP estimate, and thus an uncertainty of the TF, which can be propagated to uncertainty bounds on the TF-corrected pressure measurements and its derived quantities. Compared to the standard calibration methods, this offers an additional major advantage. Third, the disadvantage of McMC compared to a gradient-ascent with the adjoint method is that it scales badly with the number of fitting parameters. However, for the number of parameters considered for the proposed method, i.e., approximately less than 10, the scaling is not expected to pose an issue.

IV. Methodology

The specifics behind the dataset and BI method implementation are discussed in this section. The implementation and initial guess for the McMC are mentioned in Section IV.A. This is followed by a short description of the FEM simulation that serves as a benchmark dataset to the proposed method, in Section IV.B.

A. McMC implementation

For each new McMC case, a new posterior logarithmic PDF needs to be defined in the code. The McMC sampler code itself does not change from case to case. The posterior logarithmic PDF contains the prior logarithmic PDF and the W model evaluation. The latter uses code based on Eq. (2).

For this research, the parallel DRAM (ParaDRAM) McMC method of Haario et al. [28] was chosen, which is fully implemented by Shahmoradi et al. [29]. At its very base, the DRAM method is conceptually similar to the MH method, which is discussed in Section III.B. The parallelization of the sampler speeds up the method. As the sampler is fully implemented in the ParaMonte Python package [29], only the aforementioned case-specific posterior logarithmic PDF needs to be provided to the sampler by the user. The code presented by Moriaux [30] contains all required code, as well as ParaDRAM and MH examples of the proposed novel calibration approach.

For the pinhole case, built from the FEM side branch only, the initial geometry dimensions are taken from a CAD file, as visible in Fig. 3. Atmospheric parameters are set to the measured atmospheric temperature and pressure, if available, or to ISA conditions otherwise. Sutherland's law is used to estimate the dynamic viscosity, and the ideal gas law to determine the density.

The initial parameters are used both for the mean value of the prior PDF and the starting point of the Markov chain. Both extrema of the parameters are limited based on the perceived possible range of parameter values, e.g., the pinhole radius of the real-life counterpart is likely to be in the same order of magnitude as the CAD dimension.

For the McMC results presented in the paper, the random seed has been set to 3751, for the sake of repeatability. The target acceptance rate range is chosen to be 10 % to 31 %, with an adaptive update period of 50 iterations. The maximum of 30 % is a rule of thumb for the acceptance rate, balancing the number of accepted samples with the correlation between samples. For parallel methods, such as this one, a lower acceptance ratio is advised, depending on the number of processors used. Finally, the adaptation measure and autocorrelation function value provided by ParaDRAM serve to evaluate the convergence of the sampler.

B. FEM simulation dataset configuration

The pressure fluctuations inside a plane-wave calibrator of similar dimensions to that used by Van de Wyer et al. [16] and positioned on a flush-mounted microphone are simulated. The geometry is shown in Fig. 3. For the simulation, an acoustic and vibroacoustic solver is used, named NASTRAN SOL 108 (Direct Frequency Response) from Siemens Simcenter.

A total of 25 422 tetrahedral elements are used, with the smallest elements appearing in the side-branch tube at 0.7 mm, and the largest elements of 3.5 mm in the speaker cone at the upper-section of the calibrator. Considering that approximately 6 to 10 elements per wavelength are required, for the maximum element size mentioned above, the maximum achievable frequency is 16.2 kHz to 9.7 kHz.

For this dataset, the physics of the speaker in the simulation is simplified. Representing the speaker as a vibrating surface is conceptually the most accurate way. This is a feasible approach by the vibroacoustic solver. However, to achieve the correct reflections of pressure waves on the speaker-membrane surface, detailed information on the properties of the speaker membrane material is required. Instead, the speaker membrane is set as an *automatic matched layer*, i.e., an anechoic boundary. All other surfaces are set as perfectly reflective. The pressure fluctuations otherwise created by the fluctuating speaker membrane are instead induced by a monopole placed midway in the speaker cone, represented by

the red dot in Fig. 3.

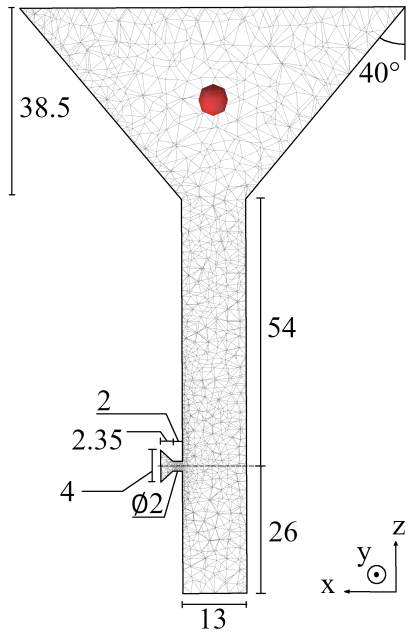

Fig. 3 Screenshot of the cross-section of the FEM geometry, which consists of cylinders and cones. The red dot in the speaker cone represents the acoustic monopole. The dimensions are provided in mm and degrees.

V. Results & Discussion

From a theoretical standpoint, the proposed semi-empirical calibration method offers a perfect fit for the frequency response of the probe being calibrated as long as the underlying analytical model for the frequency response can achieve a fitting solution. The more closely the physics underpinning the model follows the physics affecting the frequency response of the pressure probe, the better the analytical model will be able to fit the calibration data of the probe. While a theoretically sound argument, the implementation of the method is the main issue.

The logical first step is to evaluate the method in a synthetic benchmark. The FEM simulations serve as both a benchmark for the chosen analytical model and the fitting performance of the BI method. While the FEM simulation is inviscid, there is no 1-D flow assumed in the tube sections, i.e., the inverse of the W model. Therefore, this dataset is used to discuss the impact of both assumptions on the TF.

Before the method is applied to the FEM dataset, it is beneficial to investigate the resonance sources observed in the TFs in Section V.A. Only the parameters that are expected to affect the observed TF are used as fitting parameters, which speeds up the process. In Section V.B, the results of applying the method to the calibration data, which determine the feasibility of the method, are illustrated. Finally, several future improvements and features for the proposed method are mentioned in Section V.C.

A. Resonance sources of a pinhole

For standard manual post-processing techniques of calibration data, a good understanding of the expected TF of the probe is essential. While this is not strictly needed for the proposed method, it is still recommended. A good understanding of the theoretical TF of the considered probe will prevent that possible erroneous results from the proposed method are used. It will additionally speed up the convergence of the McMC towards the MAP because only the relevant fitting parameters are employed, and the convergence rate of McMC scales with the number of parameters. The underlying W model can be applied during the preliminary investigation of the TF data to analyze the effect of each parameter on the TF.

A pinhole-type RMP can be modeled with a single W-model tube-cavity element. In Section III, it is mentioned that such a geometry can be characterized by three main parameters: k_L, α, and V_v/V_t. An easy starting point is to observe

the resonance in the calibration data and understand whether it is line- or cavity resonance by seeing if the resonance has any modes or not. The TF in Fig. 4 only presents a single resonant frequency without any further modes. The nearest resonant frequency based on the CAD geometry of Fig. 3 is linked to the cavity. Hence, the resonance in the pinhole calibration data is considered to be cavity resonance. Considering the length of the pinhole, no line resonance is present within the frequency range of the calibration data. Of note in Fig. 4 is the difference in steepness of the resonant phase shift slope and peak resonance amplitude value, which is due to the viscosity of the FEM TF being extremely low compared to the conditions used for the W model. Therefore, two fitting parameters are chosen for the pinhole calibration data: V_v/V_t affects the resonant frequency of the cavity, and α affects the viscosity of the TF.

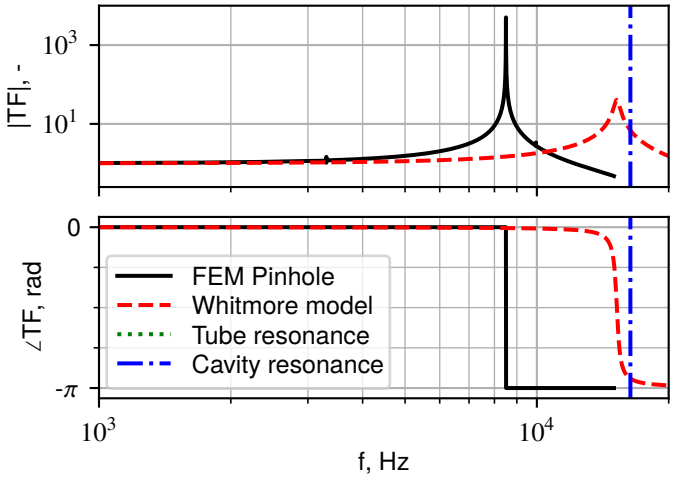

Fig. 4 FEM pinhole dataset superimposed with TF of the calibrator side-branch modeled with the W model. Resonant frequencies of half wavelength (see Eq. (4)) and Helmholtz resonator (see Eq. (5)) are overlayed. W model geometry from Fig. 3.

B. Results of the application of the method

For the proposed method to function as intended, the W model needs to converge to a good fit to the calibration data, ideally with little operator intervention.

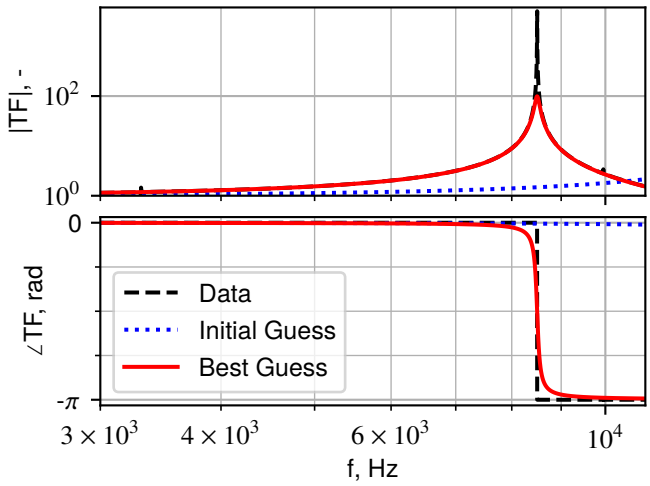

Fig. 5 TF of a pinhole from FEM simulations of the plane-wave tube geometry, used as fitting data for the W model.

The TF of the W model linked to the MAP parameters for the pinhole in Fig. 5 represent the FEM datasets well.

The resonance in the FEM data is represented by the W model. No transversal resonance modes are present in the data, and the 1-D assumption of the W model is valid. For this to be the case, the aspect ratio of the tubes must be large enough, as mentioned in Section III. Yet, a workable TF fit can be clearly achieved at much lower L/R values as well. The method might converge to effective parameter values, which differ from the geometry of the pinhole.

As mentioned before, the only major difference in the TFs of the data and the W model appears to be the shear wavenumber, which is a consequence of the FEM simulation being inviscid and the W model viscid. The results are large differences between the resonance amplitudes and phase shift slopes between the model and data at the resonant frequencies. To minimize the difference in amplitude between the data and the model around the resonant frequency, the McMC will tend to skew the overall fit. If the tube length, tube radius, and cavity volume were to be used as fitting parameters, all parameters would be strongly affected by this skewing. To reach an inviscid shear wavenumber, the radius will converge to very large values. To keep the same resonant frequency, the cavity volume will need to increase as well to maintain the same value of V_v/V_t. With the non-dimensionalized input parameters to the W model, the impact of the mismatch in viscosity only affects the shear wavenumber. To further counteract the skewing of the overall fit, some operator intervention might be required. Still, this operator intervention would be much less than that which is currently required for the manual processing of calibration data, e.g., [16], and the manual intervention would have a strongly decreased impact on the final results of the processed TF.

C. Future expansions

The above results show that the novel semi-empirical calibration approach holds much promise in providing RMP calibrations. All physical resonance is properly represented while removing spurious ones and successfully replacing them with a physically correct TF by means of the model physics. In this case, the inviscid resonance can be considered spurious to the viscid W model.

With the concept proven, further analysis of the results and improvement of the method can be considered. This further analysis is likely to come in the form of using the McMC samples to estimate the posterior PDF and looking into propagating the credible region in said PDF to the TF. To improve the fit, frequency bands in the calibration data that are problematic to the fit may be band-removed before applying the method, the prior could be altered to restrict the range of values of affected parameters, or the measurement-error standard deviation could be decreased on the TF phase data and/or increased on the TF amplitude data. In decreasing $\overline{\sigma}_d$ on the phase data compared to that on the amplitude ones, the BI places emphasis on achieving a good fit with the phase over the amplitude of the TF. And as inviscid resonance results in a smaller difference between the model and data in the phase than in the amplitude, i.e., $d - H \circ m(\overline{\alpha})$ in Eq. (7), the likelihood will be less incentivized to compromise the overall fit of the TF. These very same improvements may enable the fit not to be skewed for real calibration data with real spurious resonance [31].

Lastly, the access to all RMP parameters provided by the semi-empirical approach offers the possibility to easily apply corrective terms to the TF in a way that is simply not achievable by fully empirical calibration of RMPs. A first example of such a corrective term may be using the MAP inlet orifice radius of the probe along with the model of Corcos [7] to correct for the spatial averaging of high-frequency wall-pressure fluctuations. Another example would be to change the flow parameters in the W model while retaining all other MAP parameters to account for the impact of changes in conditions between the calibration of the RMP and the measurements with the same probe [32]. The last example would be to add onto the current model the correction for the effect of grazing flow over the RMP inlet port [33, 34].

VI. Conclusion

Unsteady pressure measurements determine, for a large part, the aeroacoustic behavior of a body submerged in a flow. RMPs, deployed to acquire these surface pressures, are typically calibrated with empirical frequency-domain dynamic techniques that can introduce spurious resonance into the calibration of the probe, which, in turn, propagates into the measurements. The research presented in this paper describes an innovative semi-empirical calibration method for RMPs that removes spurious resonance from empirical plane-wave calibrator data by fitting them with an existing analytical model for the frequency response of RMPs. The fit is performed using BI. The method has been successfully applied to a synthetic inviscid FEM dataset of a pinhole probe, which acts as a benchmark configuration for the problem under analysis. The preliminary results of this investigation already show several advantages of this approach over the current manual methods. In particular, not only the spurious resonance in the probe TF can be removed with little operator intervention, but the affected frequency band of the TF is also replaced by a physically correct alternative provided by the physics-based analytical model. Operator intervention, in both quantity and its impact on the quality of

the processed TF, is strongly reduced compared to current manual post-processing techniques of calibration data, e.g., [16, 19]. The proposed novel method delivers on its founding goal and shows further promise with regard to applying it to real calibration data with real spurious resonance [31].

Moreover, many future improvements are envisioned for the proposed method. First, the McMC can be used to provide credible regions from the posterior PDF, which can be propagated to the TF or pressure measurements to estimate the uncertainty of the calibration method. Second, multi-step calibration methods, such as performed by Van de Wyer et al. [16], may be reduced to a single calibration step. This can be achieved by fitting the model geometry of both the RMP and the calibrator to the calibration data between the RMP and the calibrator microphone of Eq. (1), and then removing the calibrator-related elements from the overall model geometry, leaving only the RMP model geometry to provide the final TF. With such a single-step calibration, the difference in the internal pressure field inside the calibrator over multiple calibration steps no longer poses an issue. This results in the fourth promising application of the method, where the single-step calibration approach can be used to provide in-situ calibration of RMPs installed in non-sealing surfaces, such as porous wall liners. As noted by dos Santos et al. [8], being able to calibrate the RMP in-situ, in the exact same configuration as during the measurements, is crucial for the accuracy of the TF, and hence the accuracy of the pressure measurements. And the interest in highly accurate unsteady pressure measurements over flow-permeable surfaces is ever-increasing with its implementation as a noise-reduction strategy for airfoils, landing gear, etc. [35–38]. Lastly, the best fit RMP parameters that result from the semi-empirical calibration form a major advantage over fully empirical calibration, as they can be used by many corrective terms for the TF or the measurements of the RMP. For example, while retaining the RMP geometrical parameters found from the fitting process, the atmospheric parameters could be altered in the model to reflect the impact of changes in the atmospheric conditions between the calibration of the RMP and the measurements performed with the same probe. Alternatively, these best-guess RMP parameters could be used in the model of Corcos [7] to account for the spatial averaging of pressure fluctuations over the finite size sensing area of the probe or, in combination with the model of Tijdeman and Bergh [33], for the impact on the TF of grazing flow over the sensing area of the probe.

In conclusion, this semi-empirical calibration is a new approach to the calibration of RMPs that not only has the potential to achieve highly accurate calibrations without spurious resonance but it opens the door to numerous future developments.

Acknowledgments

The project received funding from the European Union's Horizon 2020 research and innovation programme within the project INVENTOR (innovative design of installed airframe components for aircraft noise reduction) listed under the grant agreement ID: 860538.

References

[1] Tijdeman, H., "Investigation of the transonic flow around oscillating airfoils," Ph.D. thesis, Delft Technological University, Delft, The Netherlands, Dec. 1977. http://resolver.tudelft.nl/uuid:b07421b9-136d-494c-a161-b188e5ba1d0d.

[2] Choudhry, A., Arjomandi, M., and Kelso, R., "A study of long separation bubble on thick airfoils and its consequent effects," *International Journal of Heat and Fluid Flow*, Vol. 52, 2015, pp. 84–96. https://doi.org/10.1016/j.ijheatfluidflow.2014.12.001.

[3] Ali, S. A. S., Azarpeyvand, M., and da Silva, C. R. I., "Trailing-edge flow and noise control using porous treatments," *Journal of Fluid Mechanics*, Vol. 850, 2018, pp. 83–119. https://doi.org/10.1017/jfm.2018.430.

[4] Curle, N., "The influence of solid boundaries upon aerodynamic sound," *Proceedings of the Royal Society of London A*, Vol. 231, No. 1187, 1955, pp. 505–514. https://doi.org/10.1098/rspa.1955.0191.

[5] Bynum, D. S., Ledford, R. L., and Smotherman, W. E., "Wind tunnel pressure measuring techniques," Tech. Rep. AGARD-AG-145, North Atlantic Treaty Organization, Advisory Group for Aeronautical Research and Development, Nov. 1970. URL https://apps.dtic.mil/sti/citations/AD0714565.

[6] Peng, D., and Liu, Y., "Fast pressure-sensitive paint for understanding complex flows: from regular to harsh environments," *Experiments in Fluids*, Vol. 61, No. 1, 2019, p. 8. https://doi.org/10.1007/s00348-019-2839-6.

[7] Corcos, G. M., "Resolution of Pressure in Turbulence," *Journal of the Acoustical Society of America*, Vol. 35, No. 2, 1963, pp. 192–199. https://doi.org/10.1121/1.1918431.

[8] dos Santos, F. L., Botero-Bolívar, L., Venner, C. H., and de Santana, L. D., "Analysis of the remote microphone probe technique for the determination of turbulence quantities," *Applied Acoustics*, Vol. 208, 2023, p. 109387. https://doi.org/https://doi.org/10.1016/j.apacoust.2023.109387.

[9] Taback, I., "The Response of Pressure Measuring Systems to Oscillating Pressures," Tech. Rep. NACA-TN-1819, NACA, Langley Aeronautical Laboratory, Langley Air Force Base, Va., Feb. 1949. https://digital.library.unt.edu/ark:/67531/metadc55128/.

[10] Iberall, A. S., "Attenuation of Oscillatory Pressures in Instrument Lines," *Transactions of the American Society of Mechanical Engineers*, Vol. 72, No. 5, 2022, pp. 689–695. https://doi.org/10.1115/1.4016800.

[11] Bergh, H., and Tijdeman, H., "Theoretical and experimental results for the dynamic response of pressure measuring systems," Tech. Rep. NLR-TR F. 238, National Aerospace Laboratory NLR, Amsterdam, The Netherlands, Jan. 1965. http://resolver.tudelft.nl/uuid:e88af84e-120f-4c27-8123-3225c2acd4ad.

[12] Pierce, A. D., *Acoustics: An Introduction to Its Physical Principles and Applications*, 3rd ed., Springer Cham, Cham, Switzerland, 2019. https://doi.org/10.1007/978-3-030-11214-1.

[13] Whitmore, S. A., "Frequency response model for branched pneumatic sensing systems," *Journal of Aircraft*, Vol. 43, No. 6, 2006, pp. 1845–1853. https://doi.org/10.2514/1.20759.

[14] Whitmore, S. A., and Fox, B., "Improved accuracy, second-order response model for pressure sensing systems," *Journal of Aircraft*, Vol. 46, No. 2, 2009, pp. 491–500. https://doi.org/10.2514/1.36262.

[15] Zawodny, N. S., Liu, F., and Cattafesta, L., "Transfer matrix modeling of a recessed microphone for unsteady surface pressure measurements," *Applied Acoustics*, Vol. 117, 2017, pp. 185–190. https://doi.org/10.1016/j.apacoust.2016.10.013.

[16] Van de Wyer, N., Zapata, A., Nogueira, D., and Schram, C., "Development of a test rig for the measurement of turbulent boundary layer wall pressure statistics," *2018 AIAA/CEAS Aeroacoustics Conference*, 2018. https://doi.org/10.2514/6.2018-3122.

[17] Basten, T. G. H., and de Bree, H.-E., "Full bandwidth calibration procedure for acoustic probes containing a pressure and particle velocity sensor," *The Journal of the Acoustical Society of America*, Vol. 127, No. 1, 2010, pp. 264–270. https://doi.org/10.1121/1.3268608.

[18] Awasthi, M., Rowlands, J., Moreau, D. J., and Doolan, C. J., "Two-step hybrid calibration of remote microphones," *The Journal of the Acoustical Society of America*, Vol. 144, No. 5, 2018, pp. EL477–EL483. https://doi.org/10.1121/1.5080462, URL https://doi.org/10.1121/1.5080462.

[19] Pérennès, S., "[Aerodynamic noise sources characterization at low frequencies of high-lift devices] Caractérisation des sources de bruit aérodynamique à basses fréquences de dispositifs hypersustentateurs," Ph.D. thesis, École Centrale de Lyon, 1999. URL http://www.theses.fr/1999ECDL0032.

[20] Skilling, J., *Classic Maximum Entropy*, Springer Netherlands, Dordrecht, 1989, pp. 45–52. https://doi.org/10.1007/978-94-015-7860-8_3.

[21] Pereira, A., Antoni, J., and Leclère, Q., "Empirical Bayesian regularization of the inverse acoustic problem," *Applied Acoustics*, Vol. 97, 2015, pp. 11–29. https://doi.org/https://doi.org/10.1016/j.apacoust.2015.03.008.

[22] Azijli, I., Sciacchitano, A., Ragni, D., Palha, A., and Dwight, R. P., "A posteriori uncertainty quantification of PIV-based pressure data," *Experiments in Fluids*, Vol. 57, No. 72, 2016. https://doi.org/10.1007/s00348-016-2159-z.

[23] Tijdeman, H., "On the propagation of sound waves in cylindrical tubes," *Journal of Sound and Vibration*, Vol. 39, No. 1, 1975, pp. 1–33. https://doi.org/10.1016/S0022-460X(75)80206-9.

[24] Gumley, S. J., "A detailed design method for pneumatic tubing systems," *Journal of Wind Engineering and Industrial Aerodynamics*, Vol. 13, No. 1, 1983, pp. 441–452. https://doi.org/10.1016/0167-6105(83)90163-0.

[25] Sivia, D., and Skilling, J., *Data Analysis: A Bayesian Tutorial*, Oxford science publications, Oxford University Press, 2006.

[26] Tarantola, A., *Inverse Problem Theory and Methods for Model Parameter Estimation*, Society for Industrial and Applied Mathematics, 2005, Chaps. 3.2.2 The Least-Squares Problem: Linear Problems, pp. 64–68. https://doi.org/10.1137/1.9780898717921.

[27] van Ravenzwaaij, D., Cassey, P., and Brown, S. D., "A simple introduction to Markov Chain Monte–Carlo sampling," *Psychonomic Bulletin & Review*, Vol. 25, No. 25, 2018, p. 143–154. https://doi.org/10.3758/s13423-016-1015-8.

[28] Haario, H., Laine, M., Mira, A., and Saksman, E., "DRAM: Efficient adaptive MCMC," *Statistics and Computing*, Vol. 16, No. 4, 2006, pp. 339–354. https://doi.org/10.1007/s11222-006-9438-0.

[29] Shahmoradi, A., Bagheri, F., and Osborne, J. A., "Fast fully-reproducible serial/parallel Monte Carlo and MCMC simulations and visualizations via ParaMonte::Python library," *arXiv e-prints*, 2020, arXiv:2010.00724. URL https://ui.adsabs.harvard.edu/abs/2020arXiv201000724S.

[30] Moriaux, O., "Semi-Empirical Calibration using Bayesian inference (version 1.1)," , 2023. URL https://github.com/OMoriaux/SemiEmpiricalCalibrationBayesian.

[31] Moriaux, O., "Semi-empirical calibration of remote microphone probes using Bayesian inference," Master's thesis, Delft University of Technology, Kluyverweg 1, 2629HS Delft, South Holland, The Netherlands, 2 2023. https://doi.org/10.13140/RG.2.2.21199.97440, URL http://resolver.tudelft.nl/uuid:7cfd53ce-c443-43af-a0d3-205fa5468e8c.

[32] Samuelson, R. D., "Pneumatic instrumentation lines and their use in measuring rocket nozzle pressure," Tech. Rep. RN-DR-0124, Aerojet-General Corp., Sacramento, Calif. (USA), Jul. 1967. Doi: 10.2172/4212042.

[33] Tijdeman, H., and Bergh, H., "The influence of the main flow on the transfer function of tube-transducer systems used for unsteady pressure measurements," Tech. Rep. NLR MP 72023 U, National Aerospace Laboratory NLR, Amsterdam, The Netherlands, Sep. 1972. http://resolver.tudelft.nl/uuid:3d3e7e72-7949-4d1a-8043-3194c42edff5.

[34] Salze, E., Bailly, C., Marsden, O., Jondeau, E., and Juvé, D., "An experimental characterisation of wall pressure wavevector-frequency spectra in the presence of pressure gradients," 2014. https://doi.org/10.2514/6.2014-2909.

[35] Delfs, J., Faßmann, B., Lippitz, N., Lummer, M., Mößner, M., Müller, L., Rurkowska, K., and Uphoff, S., "SFB 880: Aeroacoustic research for low noise take-off and landing," *CEAS Aeronautical Journal*, Vol. 5, No. 4, 2014, pp. 403–417. https://doi.org/10.1007/s13272-014-0115-2.

[36] Zamponi, R., Satcunanathan, S., Moreau, S., Meinke, M., Schröder, W., and Schram, C., "Effect of porosity on Curle's dipolar sources on an aerofoil in turbulent flow," *Journal of Sound and Vibration*, Vol. 542, 2023, p. 117353. https://doi.org/10.1016/j.jsv.2022.117353.

[37] Zamponi, R., Avallone, F., Ragni, D., and van der Zwaag, S., "On the Aerodynamic-Noise Sources in a Circular Cylinder Coated with Porous Materials," *28th AIAA/CEAS Aeroacoustics 2022 Conference*, American Institute of Aeronautics and Astronautics, Southampton, UK, 2022. https://doi.org/10.2514/6.2022-3042.

[38] Zamponi, R., Gallo, E., Zarri, A., de Decker, J., Küçükosman, Y. C., and Schram, C., "Characterization of the flow through innovative permeable fairings at the VKI WAABLIEF facility," , Oct. 2022. https://doi.org/10.5281/zenodo.7220605.